Journal of Physics: Condensed
Matter

PAPER

Quantum fluctuation in thermopower at the topological phase transition in CaSrX (X: Si, Ge, Sn, Pb) studied from first principles theory

To cite this article: P C Sreeparvathy and V Kanchana 2019 *J. Phys.: Condens. Matter* **31** 095501

IOP Publishing Journal of Physics: Condensed Matter

J. Phys.: Condens. Matter **31** (2019) 095501 (10pp) https://doi.org/10.1088/1361-648X/aafa07

Quantum fluctuation in thermopower at the topological phase transition in CaSrX (X: Si, Ge, Sn, Pb) studied from first principles theory

P C Sreeparvathy and V Kanchana

Department of Physics, Indian Institute of Technology Hyderabad, Kandi—502 285, Sangareddy, Telangana, India

E-mail: kanchana@iith.ac.in

Received 27 September 2018, revised 5 December 2018
Accepted for publication 19 December 2018
Published 16 January 2019

Abstract

The present density functional calculations propose the compounds CaSrX (X: Si, Ge, Sn, Pb) as strong topological insulators, with appreciable thermoelectric properties. Emergence of Dirac semi-metallic states has been observed in CaSrX (X: Si, Ge, Sn, Pb), which is induced by uni-axial strain along '*b*' axis. CaSrSi and CaSrGe evolved as normal semiconductors with uni-axial strain. The trivial and non-trivial topological phases are evaluated by band inversion and Z_2 topological invariants. A comprehensive analysis of thermopower, electrical conductivity scaled by relaxation time at these Dirac semi-metallic states exposes the highly oscillating behaviour, which gives insight to quantum oscillations driven by uni-axial strain. Further the thermoelectric properties at strong topological insulating states and normal insulating states have been summarized, which reveals the potential thermoelectric properties of these materials.

Keywords: electronic structure, thermopower, topological materials

S Supplementary material for this article is available online

(Some figures may appear in colour only in the online journal)

1. Introduction

It has been identified that, significant number of the thermoelectric (TE) materials are having topological non-trivial states either at ambient or with some external perturbations, and Bi_2Te_3 family, transition metal chalcogenides, PbTe family and many more fall in this category [1–4]. The co-existence of TE and topological insulators (TI) properties in materials were studied previously, and was proposed that low band gap value, and complicated band profile near the Fermi level could be fruitful for both the properties [5, 6]. First principles calculations have successfully predicted significant number of TE and TI [7–9]. Both TE and TI materials are vastly in demand, where TE materials permit the conversion of waste heat to electricity and TI materials can be useful for quantum computing. The TE material capability has been quantified using figure of merit (*ZT*), which is a dimensionless quantity. $ZT = S^2\sigma T/\kappa$, where S, σ, κ, and T are the thermopower, the electrical conductivity, the thermal conductivity, and the absolute temperature, respectively. κ includes both the electronic, κ_e, and the lattice contributions, κ_l, i.e. $\kappa = \kappa_e + \kappa_l$. The highly coupled parameters in the figure of merit in general tax the efficiency of TE materials. In the case of topologically non-trivial states, the band inversion, topologically invariant parameter such as chern number, Z_2 topological invariant, and exotic surface states need to be analysed for better understanding. Strain/pressure is a prominent tool, which can tune the properties of both TE and TI materials, and there are several literatures which report that several compounds have turned from trivial to non-trivial states and vice versa as function of strain/

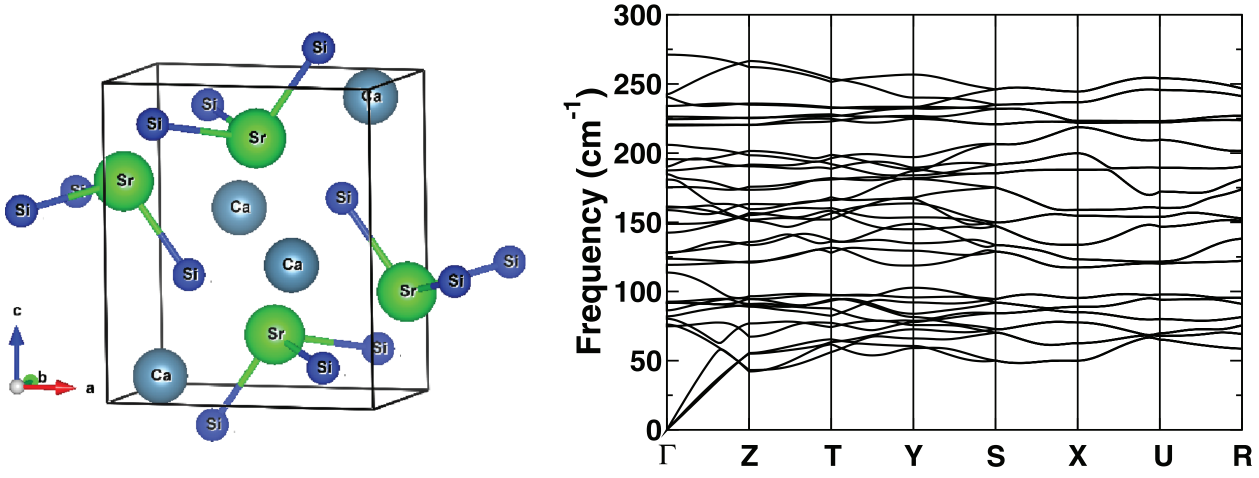

(a) (b)

Figure 1. (a) Crystal structure of the investigated compounds. (b) The phonon dispersion of CaSrSi.

pressure, which projects the importance of these calculation [10, 11]. In general the iso-structural topological transitions are possible by closing and opening the band gap, and the transition states are interesting due to the presence of Dirac/weyl semi-metallic states. Understanding of any physical properties at these states is worth doing, and needs keen attention.

In general, the thermopower is considered as a parameter for TE energy conversion, and in addition, several literatures have explored the thermopower to understand the response of the system at some exotic states [12–15]. The fluctuation of thermopower as a function of temperature has been analysed by Lu *et al* and they explored the possibility of thermopower fluctuation above superconducting temperature [14]. Later the thermopower fluctuations in the presence of magnetic filed has been connected to quantum oscillations [16]. In the recent past, the thermopower fluctuations as a function of chemical potential/carrier concentrations has been observed and studies proposed the same to be possible for quantum oscillation in thermopower in the absence of magnetic filed, and the Fermi surface topology change or strain can very well play a major role in these materials [17, 18]. From this point of view, the role of Dirac semi-metallic state, and disconnected Fermi arcs, and the relation with the thermopower fluctuation will be very interesting, and here we would like to examine the TE responses at the transition stage from a non-trivial insulators to trivial insulators. For this purpose we have analysed four zintl phase compound, which is in general shows good TE properties.

Zintl phase compounds are well recognized for possessing complex crystal structure, and are having inherent property which are helpful for TE applications [19, 20]. Significant number of zintl phase compounds fall under narrow band gap semiconductors. The huge difference in electro-negativities among the constituent elements, make these compounds more rich in chemistry. The main attraction towards these compounds is that, they generally posses high melting point and low thermal conductivity. Zintl phase compounds mostly consists of alkali, alkaline earth metals with the combination of post transition metal group elements. One of the prototype compound SrLiAs has been investigated [19], and reported as good TE material with very low thermal conductivity. The present investigated compounds are less explored, and here we wish to analyse the electronic structure, topological and TE properties of orthorhombic zintl phase compounds at ambient and as a function of strain.

Table 1. Ground state properties of CaSrX (X: Si, Ge, Sn, Pb).

Parameter	CaSrSi	CaSrGe	CaSrSn	CaSrPb
	Present			
a (Å)	7.99	8.05	8.35	8.42
a_{exp} (Å)	8.108	8.124	8.421	8.509
b (Å)	4.88	4.93	4.92	5.13
b_{exp} (Å)	4.944	4.949	5.168	5.189
c(Å)	9.18	9.24	9.71	9.79
c_{exp} (Å)	9.170	9.184	9.685	9.740
E_g (eV (with GGA))	0.37	0.40	0.27	0.09
E_g (eV (with TB-mBJ))	0.64	0.713	0.561	0.49
E_g (previous) [39] (eV (with GGA))	0.331	0.326	0.252	0.029

2. Methods

The structural optimization and phonon dispersion were calculated using plane wave self consistent field program [21], which is based on pseudo potential method. Further calculations were carried out using optimized lattice parameters. We have performed the electronic structure calculations by using WIEN2k package [22, 23], which is based on FP-LAPW (full potential linearized augmented plane wave) method. The improved band gap of investigated compounds was achieved using Tran–Blaha modified Becke–Johnson (TB-mBJ)

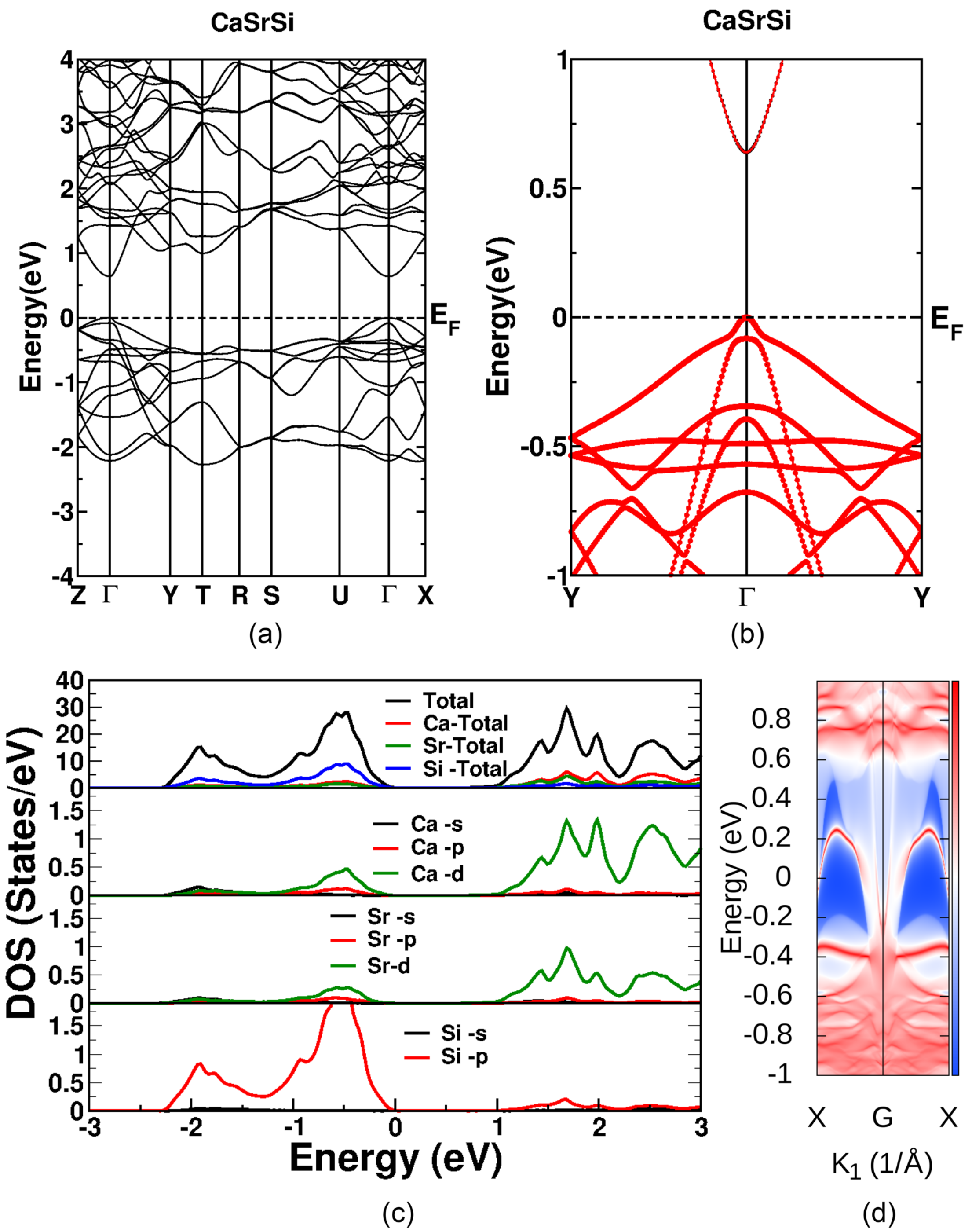

Figure 2. (a) Calculated band structure of CaSrSi, (b) projected p, d band structure of CaSrSi, the black circle represents the 'p' states, the red circle represents the 'd' states, (c) total and partial density of states for CaSrSi, (d) calculated surface spectral function along 110 surface for CaSrSi.

functional [24, 25], since the exchange correlation functional such as local density approximation and generalized gradient approximation (GGA) underestimate the band gap of semiconductors and insulators. The spin orbit effect is incorporated using second variational method in present calculations. The k-point mesh of 8 × 14 × 7 in the full Brillouin zone was used to examine the electronic properties. The BoltzTraP code [26] was used to extract the TE coefficients including thermopower (S in μV K^{-1}), electrical conductivity scaled by relaxation time (σ/τ in Ω^{-1} m^{-1} s^{-1}) with dense k-mesh. The rigid band approximation (RBA) [27–29] and the constant scattering time approximation, are incorporated in BoltzTraP code [26], and several materials have been successfully predicted using the same [30–34]. The parity analysis was performed using VASP, and all the occupied bands are taken into account for the same. Topological surface states have been calculated by combing wien2k and wannier90 package. Well converged wien2k output have been used to wannier90 and wannier-tools used to plot the spectral functions [35, 36].

3. Results and discussions

3.1. Properties at ambient conditions

The structure of the investigated compound is given in figure 1(a), and these compounds crystallize in orthorhombic structure with space group P_{nma} (62) in the form CaSrX (X: Si, Ge, Sn and Pb). The calculated ground state properties of all the investigated compounds are presented in table 1, which shows the compatibility between the present values and other reported theory and experimental values. In order to understand the electronic structure properties in detail, we have calculated the band structure with several exchange correlation functionals like GGA and TB-mBJ, together with inclusion of spin-orbit coupling in our calculation. From the analysis, we have observed that spin orbit effect is negligible in these compounds. Calculated band gaps of all the compounds are reported in table 1. For further investigation we have given the band structure along different high symmetric directions in the Brillouin zone in figure 2(a). All the compounds have almost similar band profile, and band gap value is found to be decreased from CaSrSi to CaSrPb. The band gap is found to be direct at Γ high symmetry point. Along all crystallographic directions such as a–c the bands are found to be dispersive in the valence band, and along 'b' axis the dispersion is little higher compared to other two directions. In the conduction band also, the scenario is same. The band along R-S is found to highly flat in the valence band. A thorough analysis of the band structure of CaSrSi reveals a highly linearized Dirac like band profile along $\Gamma - Y$ direction in conduction band. Figure 2(b) represents the projected bands structure, which confirm the domination of Si-p states near valence band and a competing Si-p and Sr-d states in the conduction band.

The calculated elastic constants of all the investigated compound are presented in table 2. All the elastic constants for all the compounds are found to be positive and found to preserve the born stability criteria, confirming the mechanical stability of these compounds. The range of values for the elastic constants are comparable with prototype materials. Calculated bulk modulus and Debye temperature of all the compounds are also given in table 2. The magnitude of Debye temperature is found to be decreased from Si to Pb. In addition, the dynamical stability has been verified through phonon dispersion, and the same for CaSrSi is given in figure 1(b). The flat nature of phonon dispersion of all the investigated compounds indicate the possibility of low thermal conductivity in these set of compounds. From figure 1(b) it is quite clear that the interaction of acoustic and optical modes are found below 70 cm^{-1} for all the investigated compound. The possibility for low thermal conductivity value is highly fruitful for TE applications.

The peculiar band profile along $\Gamma - Y$ direction motivate us to analyse the topological nature of these compounds. All these compounds preserve time reversal symmetry, and Z_2 topological invariant can be examined to understand the topological character. In addition, the system possesses inversion symmetry and these space group also fall into non-symmorphic crystalline group. Due to the combination of time reversal symmetry and inversion symmetry, Z_2 topological invariant can be calculated from the parity of bands in each TRIM point (time reversal invariant momentum) in the Brillouin zone. Here we have to consider the case of three dimensional system, in which the system possess 8 TRIM points, which are $(0,0,0), (0.5,0,0), (0.0,0.5,0.0), (0.0,0.0,0.5), (0.5,0.5,0.0), (0.5,0.0,0.5), (0.0,0.5,0.5)$ and $(0.5,0.5,0.5)$. For this purpose we have adapted the method suggested by Fu and Kane [37]. The equation for Z_2 topological invariant is, $(-1)^\nu = \prod \gamma_i$ where γ_i are parities of each band. Calculated Z_2 topological invariants of all the compounds are represented in table 3. Since these compounds are semiconductors, we have considered all the occupied bands for the calculations, and we have found that at Γ point, parity is -1 and all the other points the value is $+1$, and lead to a non zero value for Z_2 parameter. All the investigated compounds are found to be strong TIs. Further we have calculated the surface states for all the compounds and calculated surface state of CaSrSi is presented in figure 2(d). Highly linearized Dirac cone like surface bands is observd around Γ high symmetry point, which again confirm the strong topological nature in this compound, similar surface states are observed for all the compounds which is given in supplementary figure S1 (stacks.iop.org/JPhysCM/31/095501/mmedia). In the next section we deal with the TE properties of these compounds.

Table 2. Calculated elastic constants of CaSrX (X: Si, Ge, Sn, Pb).

	CaSrSi	CaSrGe	CaSrSn	CaSrPb
	Present			
C_{11} (GPa)	68.72	64.58	57.17	53.98
C_{22} (GPa)	77.23	74.64	66.35	61.99
C_{33} (GPa)	73.52	69.37	62.19	59.15
C_{44} (GPa)	35.23	34.02	29.69	28.27
C_{55} (GPa)	28.98	27.89	23.54	22.06
C_{66} (GPa)	34.11	32.58	28.10	26.33
C_{12} (GPa)	19.85	19.01	17.52	16.94
C_{13} (GPa)	19.24	17.83	15.44	14.39
C_{23} (GPa)	22.53	20.23	19.16	17.38
Debye T(K)	340.79	295.44	253.82	212.41

Table 3. Calculated Z_2 topological invariants of CaSrX (X: Si, Ge, Sn, Pb) at ambient.

	CaSrSi	CaSrGe	CaSrSn	CaSrPb
ν_0	1	1	1	1
ν_1	0	0	0	0
ν_2	1	1	1	1
ν_3	0	0	0	0

TE properties such as thermopower, electrical conductivity scaled by relaxation time (will be address as electrical conductivity) and power-factor as a function of carrier concentrations at different temperatures are analysed for all the compounds. Figures 3(a) and (b) represent the thermopower for CaSrSi as a function of both hole and electron concentrations at different temperatures. The difference in band dispersion along

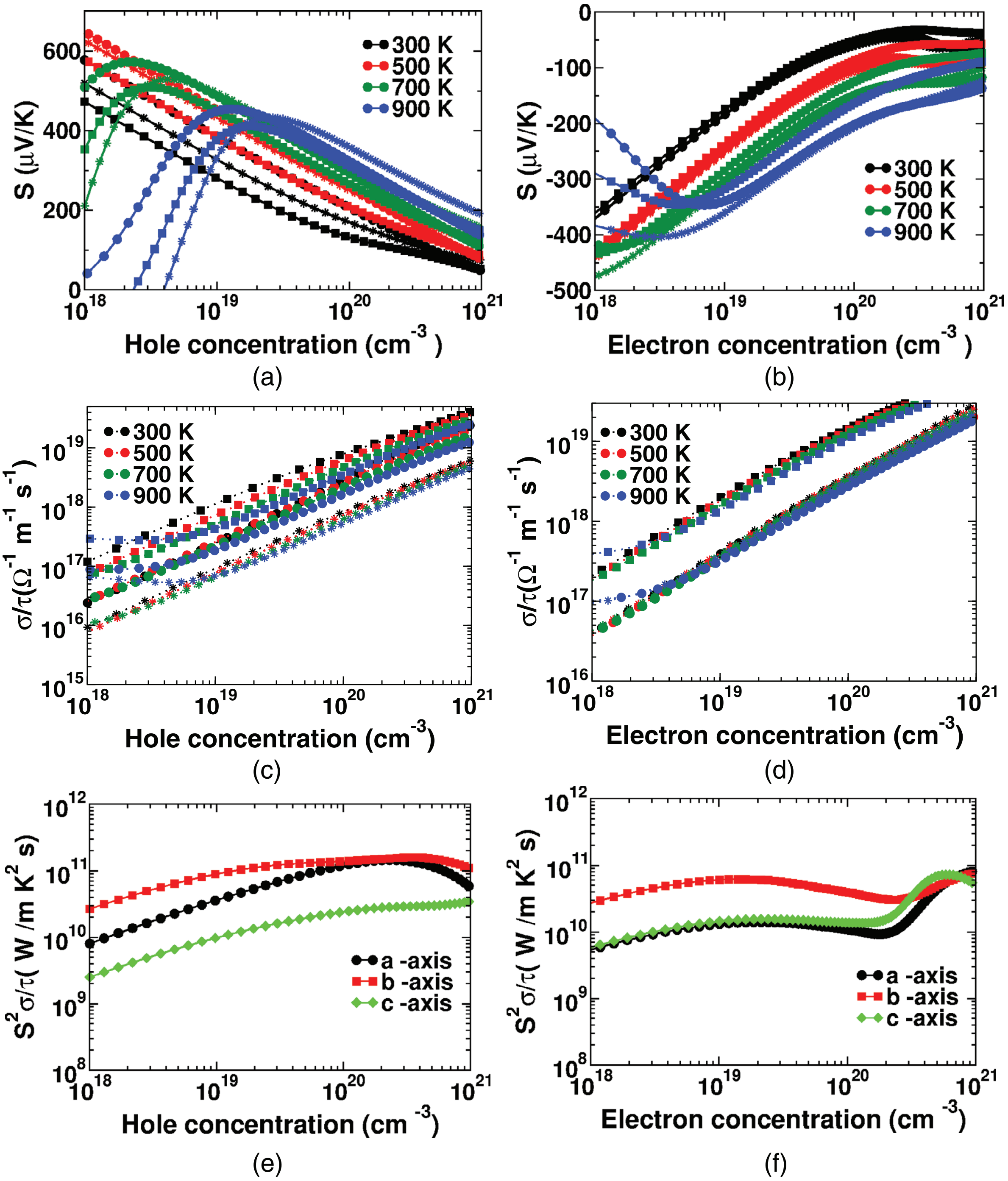

(a) (b) (c) (d) (e) (f)

Figure 3. Calculated TE properties for CaSrSi at different temperatures, (a) thermopower as a function of hole concentration, (b) thermopower as a function of electron concentration, (c) electrical conductivity scaled by relaxation time as a function of hole concentration, (d) electrical conductivity scaled by relaxation time as a function of electron concentration, (e) power factor as a function of hole concentration, (f) power factor as a function of electron concentration.

different crystallographic directions are reflected in thermopower. Around 300 K, thermopower along '*a*' axis has secured the highest value than '*c*'-axis value and followed by '*b*'-axis value. When we move to higher temperature the difference between '*a*'-axis and '*c*'-axis values are reducing, and '*b*'-axis value remains the lowest. Around 700 K onwards bipolar conduction has been seen for low concentration range. Coming to electron doping, the thermopower values are more isotropic and bipolar conduction is observed same as that of holes. The magnitude of thermopower for electron doping is lesser than the same for hole doping. Figures 3(c) and (d) present the electrical conductivity for CaSrSi for both holes and electrons at different temperatures. At around 300 K, conductivity along '*b*'-axis is found to be more, and '*c*'-axis has the lowest value. Up to 700 K the trend is same, and around 900 K at low concentrations, the conductivity is found to be invariant as a function of carrier concentration, and for higher concentrations it varies linearly. In the case of electron doping, for

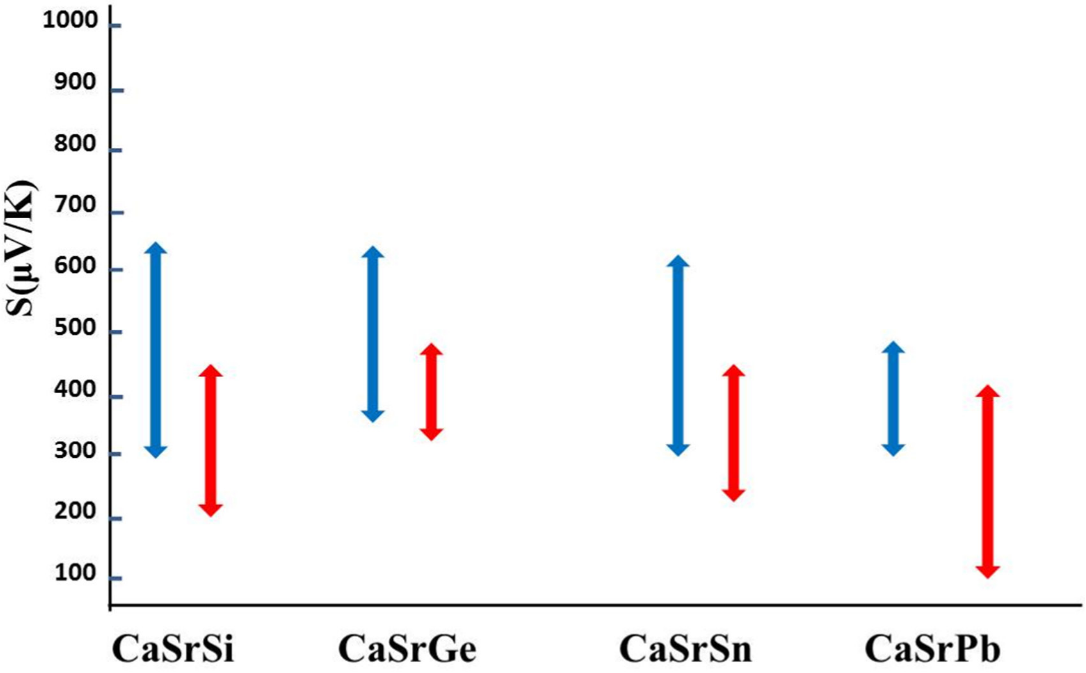

Figure 4. Magnitude of thermopower for both holes and electrons over the temperature range 100 K–500 K for all the compounds, blue colour represents hole thermopower, red colour represents electron thermopower.

all temperatures the *b*-axis value is higher, and other two axes values are found to be almost same. Power factor of CaSrSi is presented in figures 3(e) and (f). For hole doping, significant difference is observed between each crystallographic directions, and '*b*'-axis is found to have highest value. But for electron doping, we can see a kind of anisotropic character, where *b*-axis value is higher than '*a*' and '*c*' axes. Since all the investigated compounds show bipolar conduction at higher temperatures, we have presented the magnitude of thermopower over a temperature range 100 K–500 K around the carrier concentration of 10^{18} cm^{-3} for all the compounds in figure 4. From the figure it is quite evident that, all the investigated compounds possess an appreciable value of thermopower over the temperature range of 100 K–500 K. Electrical conductivity and power-factor of other compounds also found to show similar behaviour as that of CaSrSi. The variation of electrical conductivity as a function of both hole and electron concentration for different temperatures for all the other compounds are presented in supplementary figure S2. As we mentioned earlier, the figure of merit is an important paramater for TE materials. The magnitude of power-factor for all the compounds at 300 K around the concentration range 10^{19} cm^{-3} is around 1×10^{11}, which is apreciable. Another vital parameter is the thermal conductivity, and here we have calculated the minimum lattice thermal conductivity of all the compounds using Cahill's modal [38]. Calculated minimum thermal conductivity for CaSrSi, CaSrGe, CaSrSn and CaSrPb are 0.328, 0.258, 0.222 and 0.192 W mK^{-1} respectively. From our earlier discussions, we have mentioned that the low value of Debye temperature and flat phonon bands might cause for low thermal conductivity. Further we have assumed the relaxation time as 10^{-14} s, and calculated the range of the figure of merit for all the compounds at 300 K. The calculated value of the figure of merit at 300 K for CaSrSi, CaSrGe, CaSrSn and CaSrPn are 1.34, 1.5, 1.48 and 1.68 respectively. Altogether the present study reveals the topologically non-trivial states and presented noticeable TE properties of all the investigated compounds at ambient. Subsequently we have analysed the effect of strain, which is presented in the upcoming section.

3.2. *Effect of strain*

In general TIs are very sensitive to external perturbations such as strain/pressure. In the present study, we have analysed the strain effects on electronic topological nature and transport properties. First we have applied hydrostatic compressive and tensile strain to these system, and band gap of all the compounds is found to reduce with compressive strain and found to be increased with tensile strain. The band profile is preserved for these hydrostatic strain. Further we have applied uni-axial strain along different crystallographic directions, and found drastic changes in band profile. Among the three axes, the uni-axial strain applied along '*b*' axis is found to have more impact on the electronic and hence on transport properties of the investigated compounds. Starting the discussion with the compressive strain on CaSrSi, a drastic change has been observed in the band profile of CaSrSi. Figures 5(a)–(d) represents the band structure along the high symmetry direction $T - \Gamma - Y$ and $U - \Gamma - X$ at different compressive strains, The band gap is found to be decreased and closed around -10% and then opens again around -12% strain. Here Γ is the centre of the *BZ*, *T* is in '*yz*' plane (0.0, 0.5, 0.5), *Y* is along '*y*' axis (0.0, 0.5, 0), then the first path $T - \Gamma - Y$ in in '*YZ*' plane. Likewise *U* point is lying in '*xz*' plane (0.5, 0, 0.5), and *X* is along '*x*' axis, and the second path is in '*XZ*' plane. As we mentioned earlier the band gap is found to be reduced and the band profile has

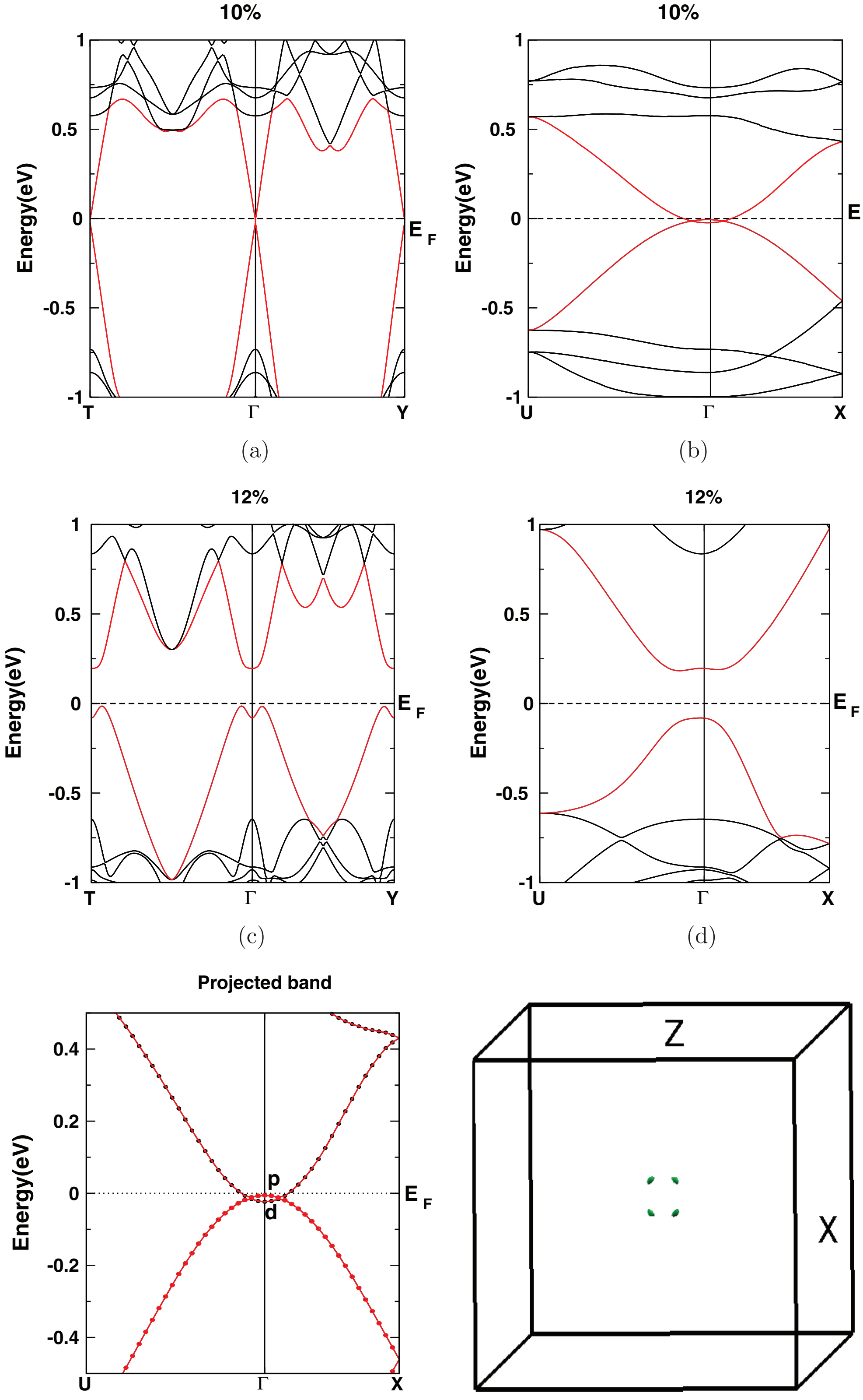

(a) (b) (c) (d) (e) (f)

Figure 5. (a) Band structure of CaSrSi at 10% compressive strain along 'b' axis in $T - \Gamma - Y$ direction, (b) band structure of CaSrSi at 10% compressive strain along 'b' axis in $U - \Gamma - X$ direction, (c) band structure of CaSrSi at 12% compressive strain along 'b' axis in $T - \Gamma - Y$ direction, (d) band structure of CaSrSi at 12% compressive strain along 'b' axis in $U - \Gamma - X$ direction, (e) 'p' and 'd' projected band structure at 10% strain, (f) Fermi surface of CaSrSi at 10% compressive strain.

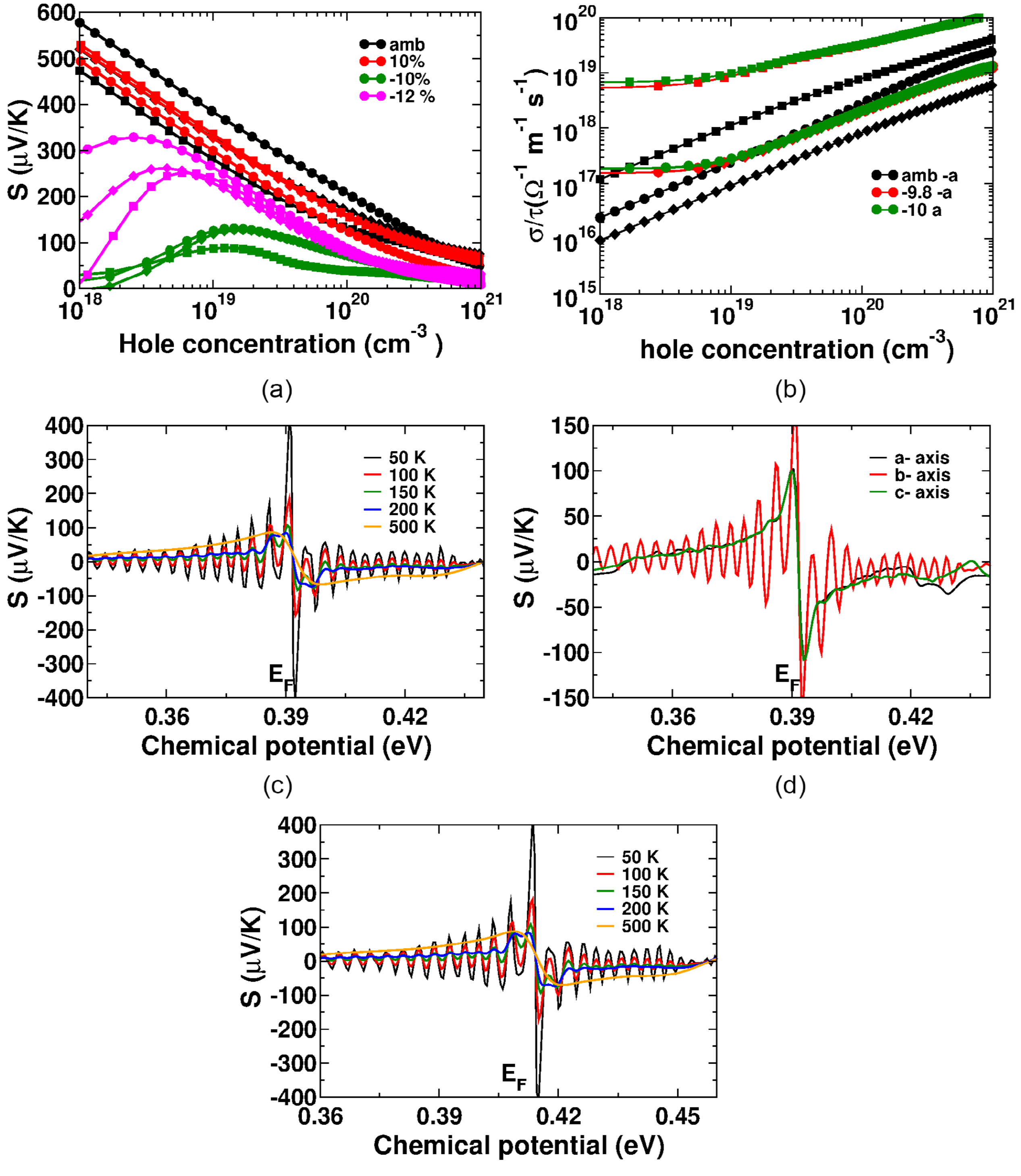

(a) (b)

(c) (d)

(e)

Figure 6. (a) Variation of thermopower as a function of hole concentration for different strains, (b) variation of electrical conductivity scaled by relaxation time as a function of hole concentration for different strains, (c) thermpower variation as a function of chemical potential for CaSrSi at 10% compressive strain along '*b*' axis at different temperatures, (d) thermpower variation as a function of chemical potential for different crystallographic directions for CaSrSi at 10% compressive strain at 100 K, (e) thermpower variation as a function of chemical potential for CaSrGe at 11% compressive strain along '*b*' axis at different temperatures.

been changed. Let us see the case from 6% compressive strain onward (see supplementary figure S3). The ambient and 6% are almost the same and around 8% onwards the bands gets more linearized and then at 10% strain, an exactly Dirac like cone is observed. Around 12%, the linear dispersion nature has vanished, and a double well kind of band profile along $\Gamma - Y$ is seen. On the other hand, the high symmetric direction $U - \Gamma - X$ preserved a parabolic nature as a function of compressive strain and around 10%, the conduction and valence band touch each other and then opens the band gap around 11%. From these analyses we could see that, the band dispersion along *YZ* plane and *ZX* plane is completely different. The closing and opening of band gap nature motivated us to verify the Z_2 topological invariant in these strained states. Our calculations suggest that CaSrSi is converting to a normal insulator through *b*-axis uni-axial compressive strain, where the parity at Γ point has found to be flipped to +1, which give a zero Z_2 value. The projected band structure clearly shows that, the band flipping is happening between Sr-d and Si -p states (see figure 5(e)), which further provides the confirmation for the transformation from a strong topological insulating state to a normal insulating state. Similar behaviour we have observed in CaSrGe also, for that the band closing is found around 11% compressive strain, the band structure of the same is given in supplementary data (see figure S4). The remaining compounds CaSrSn and CaSrPb preserve their non-trivial states up to 15% '*b*' axial compressive strain. For further strain, these compounds also might show similar behaviour. With uni-axial tensile strain along '*b*' axis, the band gap is found to increase. For compressive strain (uni-axial strain along '*b*' axis) around 10%, the band gap is found to be closed and the system turned to a semi-metallic state, and the Fermi surface formed in this state is very interesting (see figure 5(d)). An extremely small arc has been observed in the '*XZ*' plane, which is due to the parabolic bands present there. This small arc-like Fermi surface provides further information about the dimensional reduction in the system. It has to be noted that the uni-axial strain along the other two axes are also studied, where we could not observe many interesting properties within the applied strain. For further strain, these directions also might show similar trends.

In the previous section, we discussed the changes in electronic structure with respect to strain along different directions. Further, we have analysed the TE properties of investigated compounds as a function of hydrostatic and uni-axial strain along different directions. The thermopower for CaSrSi as a function of carrier concentration at different hydrostatic strains is presented in supplementary data (see figures S5(a) and (b)). The magnitude of thermopower is found to be reduced with compressive strain and found to be increased with tensile strain. In the case of electrical conductivity, we can see reverse trends, and for electron doping we can see the anisotropy in electrical conductivity (see figures S4(c) and (d)).

In figure 6(a), we have given the thermopower variation as a function of '*b*' axis strain. From the electronic structure, we could see that, CaSrSi transfer to a semi-metallic state around −10% compressive strain, and in that state the thermopower is found to be very low. For further strain around −12%, the thermopower values are found to be increased again, which is according to the band opening in this state. For tensile strain, the magnitude of thermopower is found to be comparable with the ambient value, and anisotropy in thermopower is found to be reduced. Electrical conductivity for compressive strain along the '*b*' axis is found to enhance the magnitude of anisotropy in the system (see figure 6(b)). Above −9.5% strain, the system is found to possess huge anisotropy, where conductivity values along '*b*' axes is found to be two orders higher than '*a*' and '*c*' axes. This indicates a quasi two-dimensional nature in the system.

As we discussed in the previous sections, the compressive strained state along '*b*' axis (around 10%) has shown several interesting phenomena for CaSrSi. In this state, the system turned to be a metallic state, with remarkable electronic structure which included a highly Dirac cone-like band structure along the $\Gamma - Y$ direction, and parabolic bands along the perpendicular plane. The huge difference in the band dispersion along these directions, which is induced by strain has become root for peculiar transport properties at this state. We have observed a highly interesting transport response at these strained state around −10% at low temperatures around the range 50 K–150 K along '*b*' axes. Here the nature of thermopower along '*a*' and '*c*' axes are found to be quite normal, and the '*b*' axis' thermopower shows a highly oscillating variation as a function of chemical potential/carrier concentrations, which is represented in figure 6(c). The small disconnected arc-like Fermi surface also supports this behaviour. This strained state is the transition state between a strong TI insulator to a normal insulator. As we mentioned in the introduction part, the thermopower fluctuation can originate from several ways with or without a magnetic field [12–15]. Here we would like to address this thermopower fluctuation as quantum oscillations, which might be originating through the application of strain. One vital point here is that, as this strained state system is almost two dimensional, which again gives strong insight to our observation, where these kind of quantum fluctuations in physical quantities can be expected. In the case of CaSrGe also we could see similar behaviour, which is presented in figure 6(e).

While concluding, we throw light for further discussion regarding the abnormal behaviour of thermopower along '*b*' axis, which can be verified by the experimentalists.

4. Conclusions

A systematic analysis of electronic, topological and transport properties were presented, and identified the studied materials as TIs at ambient conditions. The potential TE properties were also presented for the investigated compounds. The application of strain in these systems gave insight into several interesting phenomena, which include the formation of a Dirac semi-metallic state, and quantum fluctuation in thermopower with an enhanced 2D nature, which opens up a wide application range for the investigated compounds.

Acknowledgment

The authors SPC and VK would like to thank IIT Hyderabad and National PARAM Supercomputing Facility (NPSF) and Centre for Development of Advanced Computing (C-DAC), Pune for computational facility and SPC would like to thank MHRD for fellowship.

ORCID iDs

V Kanchana https://orcid.org/0000-0003-1575-9936

References

[1] Zhang H *et al* 2009 *Nat. Phys.* **5** 438
[2] Zhang M *et al* 2018 *Phys. Lett.* A **382** 673
[3] Yang G, Liu J, Fu L, Duan W and Liu C 2014 *Phys. Rev.* B **89** 085312
[4] Feng W *et al* 2011 *Phys. Rev. Lett.* **106** 016402
[5] Xu Y, Gan Z and Zhang S 2014 *Phys. Rev. Lett.* **112** 226801
[6] Mchler L *et al* 2013 *Phys. Status Solidi RRL* **7** 91
[7] Gudelli V K, Kanchana V and Vaitheeswaran G 2016 *J. Phys.: Condens. Matter* **28** 025502
[8] Fan T, Xie C, Wang S, Oganov A R and Cheng L 2018 *RSC Adv.* **8** 17168
[9] Ma Y, Dai Y, Kou L, Frauenheim T and Heine T 2015 *Nano Lett.* **15** 1083
[10] Ochi M, Arita R, Trivedi N and Okamoto S 2016 *Phys. Rev.* B **93** 195149
[11] Zhang M, Wang1 X, Rahman A, Zeng Q, Huang D, Dai R, Wang Z and Zhang Z 2018 *Appl. Phys. Lett.* **112** 041907
[12] Daou R, Frsard R, Hbert S and Maignan A 2015 *Phys. Rev.* B **92** 245115
[13] Dubi Y 2013 *New J. Phys.* **15** 105004
[14] Lut Y and Patton B R I 1995 *J. Phys.: Candens. Matter* **7** 9247
[15] Gallagher B L *et al* 1990 *Phys. Rev. Lett.* **64** 2015
[16] Matusiak M and Cooper J R 2017 *Nat. Commun.* **8** 15219
[17] Liu T, Pikulin D I and Franz M 2017 *Phys. Rev.* B **95** 041201
[18] Rossi E, Bardarson J H, Fuhrer M S and Das Sarma S 2012 *Phys. Rev. Lett.* **109** 096801
[19] Guo L B, Wang Y X, Yan Yu L, Yang G, Yang J M and Feng Z Z 2014 *J. Appl. Phys.* **116** 033705
[20] Khan S A and Reshak A H 2014 *Comput. Mater. Sci.* **95** 328
[21] Giannozzi P *et al* 2009 *J. Phys.: Condens. Matter* **21** 395502
[22] Blaha P, Schwarz K, Madsen G K H, Kvasnicka D, Laskowski R, Tran F and Marks L D 2018 WIEN2k, An Augmented Plane Wave + Local Orbitals Program for Calculating Crystal Properties (Karlheinz Schwarz, Techn. Universität Wien, Austria)
[23] Blaha P, Schwarz K, Sorantin P I and Tricky S B 1990 *Comput. Phys. Commun.* **59** 399
[24] Becke A D and Johnson E R 2006 *J. Chem. Phys.* **124** 221101
[25] Tran F and Blaha P 2009 *Phys. Rev. Lett.* **102** 226401
[26] Madsen G K H and Singh D J 2006 *Comput. Phys. Commun.* **175** 67
[27] Scheidemantel T J, Ambrosch-Draxl C, Thonhauser T, Badding J V and Sofo J O 2003 *Phys. Rev.* B **68** 125210
[28] Jodin L, Tobola J, Pecheur P, Scherrer H and Kaprzyk S 2004 *Phys. Rev.* B **70** 184207
[29] Chaput L, Pecheur P, Tobola J and Scherrer H 2005 *Phys. Rev.* B **72** 085126
[30] Ong K P, Singh D J and Wu P 2011 *Phys. Rev.* B **83** 115110
[31] Singh D J and Mazin I I 1997 *Phys. Rev.* B **56** R1650
[32] Parker D and Singh D J 2010 *Phys. Rev.* B **82** 035204
[33] Madsen G K H, Schwarz K, Blaha P and Singh D J 2003 *Phys. Rev.* B **68** 125212
[34] Zhang L, Du M-H and Singh D J 2010 *Phys. Rev.* B **81** 075117
[35] Sancho M P L, Sancho J M L and Rubio J 1984 *J. Phys. F: Met. Phys.* **14** 1205
[36] QuanSheng W, Zhang S N, Song H-F, Troyer M and Soluyanov A A 2018 *Comput. Phys. Commun.* **224** 405
[37] Fu L and Kane C L 2007 *Phys. Rev.* B **76** 045302
[38] Cahill D G, Watson S K and Pohl R O 1992 *Phys. Rev.* B **46** 6131
[39] Saoudi A *et al* 2012 *Solid State Commun.* **152** 1800–6